Author Manuscript

Author Manuscript

Author Manuscript

Author Manuscript

HHS Public Access

Author manuscript

*Adv Mater*. Author manuscript; available in PMC 2017 May 01.

Published in final edited form as:

*Adv Mater*. 2016 May ; 28(17): 3273–3279. doi:10.1002/adma.201505700.

# Multimodal Imaging Guided Cancer Phototherapy by Versatile Biomimetic Theranostics with UV and γ Irradiation Protection

**Dr. Jing Lin**,
Guangdong Key Laboratory for Biomedical Measurements and Ultrasound Imaging, Department of Biomedical Engineering, School of Medicine, Shenzhen University, Shenzhen 518060, China

Laboratory of Cellular Imaging and Macromolecular Biophysics, National Institute of Biomedical Imaging and Bioengineering (NIBIB), National Institutes of Health, Bethesda, Maryland 20892, United States

**Min Wang**,
State Key Laboratory of Cancer Biology, Xijing Hospital of Digestive Diseases, Fourth Military Medical University, Xi'an 710032, China

**Dr. Hao Hu**,
Laboratory of Molecular Imaging and Nanomedicine (LOMIN), National Institute of Biomedical Imaging and Bioengineering (NIBIB), National Institutes of Health, Bethesda, Maryland 20892, United States

State Key Laboratory of Cancer Biology, Xijing Hospital of Digestive Diseases, Fourth Military Medical University, Xi'an 710032, China

**Xiangyu Yang**,
Laboratory of Molecular Imaging and Nanomedicine (LOMIN), National Institute of Biomedical Imaging and Bioengineering (NIBIB), National Institutes of Health, Bethesda, Maryland 20892, United States

**Bronte Wen**,
Laboratory of Molecular Imaging and Nanomedicine (LOMIN), National Institute of Biomedical Imaging and Bioengineering (NIBIB), National Institutes of Health, Bethesda, Maryland 20892, United States

**Zhantong Wang**,
Laboratory of Molecular Imaging and Nanomedicine (LOMIN), National Institute of Biomedical Imaging and Bioengineering (NIBIB), National Institutes of Health, Bethesda, Maryland 20892, United States

**Dr. Orit Jacobson**,
Laboratory of Molecular Imaging and Nanomedicine (LOMIN), National Institute of Biomedical Imaging and Bioengineering (NIBIB), National Institutes of Health, Bethesda, Maryland 20892, United States

**Dr. Jibin Song**,

Correspondence to: Peng Huang, peng.huang@szu.edu.cn; Xiaoyuan Chen, shawn.chen@nih.gov.

Author Manuscript Author Manuscript Author Manuscript Author Manuscript

Laboratory of Molecular Imaging and Nanomedicine (LOMIN), National Institute of Biomedical Imaging and Bioengineering (NIBIB), National Institutes of Health, Bethesda, Maryland 20892, United States

**Dr. Guofeng Zhang**,
Laboratory of Cellular Imaging and Macromolecular Biophysics, National Institute of Biomedical Imaging and Bioengineering (NIBIB), National Institutes of Health, Bethesda, Maryland 20892, United States

**Dr. Gang Niu**,
Laboratory of Molecular Imaging and Nanomedicine (LOMIN), National Institute of Biomedical Imaging and Bioengineering (NIBIB), National Institutes of Health, Bethesda, Maryland 20892, United States

**Prof. Peng Huang**, and
Guangdong Key Laboratory for Biomedical Measurements and Ultrasound Imaging, Department of Biomedical Engineering, School of Medicine, Shenzhen University, Shenzhen 518060, China

**Prof. Xiaoyuan Chen**
Laboratory of Molecular Imaging and Nanomedicine (LOMIN), National Institute of Biomedical Imaging and Bioengineering (NIBIB), National Institutes of Health, Bethesda, Maryland 20892, United States

Peng Huang: peng.huang@szu.edu.cn; Xiaoyuan Chen: shawn.chen@nih.gov

## TOC image

We have developed a versatile biomimetic theranostic agent based on magnetic melanin nanoparticles (MMNs) for positron emission tomography (PET)/magnetic resonance (MR)/ photoacoustic (PA)/photothermal (PT) multimodal imaging guided cancer photothermal therapy (PTT), UV and γ irradiation protection.

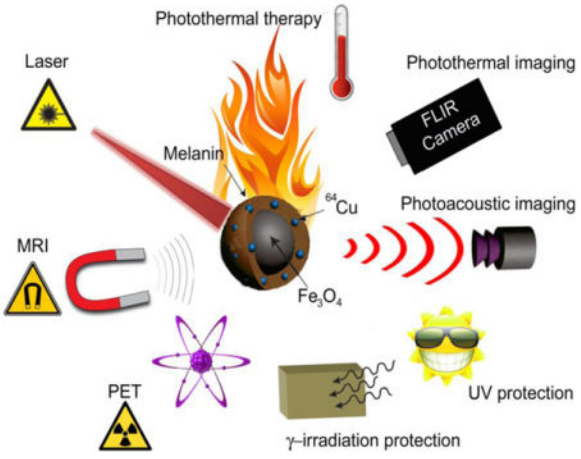


### Keywords

Theranostics; melanin; iron oxide; biomimetic synthesis; PET; MRI; photoacoustic imaging; photothermal therapy; UV protection; γ protection

Author Manuscript Author Manuscript Author Manuscript Author Manuscript

Activatable theranostics fight against diseases through the combination of diagnostic and therapeutic moieties.[1] With the rapid development of biomedical imaging techniques, multimodality imaging provides complementary information by integrating information from various imaging modalities, gaining increasing recognition as a more accurate diagnostic technique than any single imaging modality alone.[2] To date, PET/CT (positron emission tomography/X-ray computed tomography) and PET/MRI (magnetic resonance imaging) have found wide-spread clinical use, which further stimulates the development and construction of efficient multimodal contrast agents with multi-response capacity under different imaging techniques.

Iron oxide (IO) nanoparticles, due to their intrinsic magnetic property, have been widely employed as building blocks for the construction of contrast agents to achieve multimodality imaging,[3] such as MRI/FL (fluorescence),[4] MRI/CT, MRI–PET/SPECT (single-photon emission computed tomography),[5] MRI/PET/FL,[6] MRI/CT/FL,[7] MRI/PET/FL/BLI (bioluminescence),[8] MRI/MPI (magnetic particle imaging),[9] magneto-motive ultrasound imaging (MMUS),[10] and magneto-photoacoustic imaging (MPA).[11] Their MR contrast effect can be improved to achieve highly sensitive MRI by controlling their size, shape, and composition.[2a] However, IO nanoparticles functionalized with most types of materials (e.g. fluorescent molecules and radioisotopes) mostly weakens their MR contrast effect.[2a] Therefore, the development of novel IO-based multimodal contrast agents with enhanced MR contrast is highly desirable for optimizing MRI and other imaging modalities.

Inspired by the fascinating characteristics of melanin, such as i) high brightness on $T_1$-weighted images and darkness on $T_2$-weighted images;[12] ii) high affinity for metal ions, especially copper, iron, manganese, and zinc;[13] iii) strong absorbance in the near-infrared (NIR) region;[14] iv) good biodegradability and biocompatibility;[14] we therefore strategically designed and synthesized radionuclide $^{64}$Cu-labeled magnetic melanin nanopaticles ($^{64}$Cu-MMNs) by biomimetic synthesis method using biopolymer melanin as the biotemplate. The radionuclide $^{64}$Cu was coupled with MMNs through the strong affinity of copper ions to melanin for PET imaging. Meanwhile, the unique superparamagetism and strong NIR absorbance of MMNs are used for enhanced MRI and photoacoustic (PA)/ photothermal (PT) imaging, respectively. Based on the PET/MR/PA/PT multimodal imaging guidance, the photoactive hyperthermia effect of MMNs upon 808 nm laser irradiation can be used for photothermal therapy (PTT). Most intriguingly, MMNs also exhibit efficient shielding against UV and γ irradiation. The as-prepared $^{64}$Cu-MMNs were investigated as a versatile biomimetic theranostic agent for PET/MR/PA/PT multimodal imaging guided PTT, UV and γ irradiation protection for the first time (Figure 1a).

The MMNs were prepared by a biomimetic synthesis method using melanin to direct the co-precipitation of $Fe^{3+}$ and $Fe^{2+}$ ions (molar ratio at 2:1) under alkaline condition. The as-prepared MMNs showed well-defined spherical morphology with the diameter around 15 nm (Figure 1b). The hydrodynamic diameter of MMNs was 61.8 ± 18.9 nm (PDI = 1.201), which was measured by the dynamic light scattering (DLS) method (Figure 1c). The difference in diameter was ascribed to the melanin coating layer. As shown in the UV-vis-NIR absorption spectra (Figure 1d), MMNs showed concentration-dependent absorbance increase in the NIR region, with a good linear relationship of optical density at 808 nm

Author Manuscript Author Manuscript Author Manuscript Author Manuscript

versus its concentration, described by the following typical equation: $Y = 0.00116 + 0.002X$ ($R^2 = 0.9998$) (Figure S1). By adjusting the amount of melanin, the surface melanin density of MMNs was well controlled, showing a melanin density-dependent negative charge decrease that implied more and more binding sites for copper ions (Figure S2).

Based on melanin's high affinity tofor copper ion,[13a] MMNs were successfully radiolabeled with isotope $^{64}$Cu through simple mixing. After 1 h incubation, the labeling efficiency was measured by instant thin layer chromatography (iTLC) with saline as the eluant (Figure 2a–c). The radiochemical yield of MMNs was ~100% (Figure 2a). Magnetic nanopaticles (MNPs) without melanin showed very low labeling efficiency (Figure 2c). The enhanced MR effect of MMNs was investigated. As shown in the inset of Figure 2d, darker $T_2$-weighted MRI images of the aqueous solutions of MMNs were observed with increased MMN concentration. The slope, as given by the $r_2$ value, was evaluated to be 167.28 $mM^{-1}$ $s^{-1}$(Figure 2d), which was much higher than those of MNPs (76.48 $mM^{-1}$ $s^{-1}$) (Figure S3) and the commercial MNPs (10 nm, $r_2 = 59.91 \pm 6$ $mM^{-1}$ $s^{-1}$ and 16 nm, $r_2 = 125.86 \pm 9$ $mM^{-1}$ $s^{-1}$)[15] (Figure 2e). The PA signal intensities were linearly correlated with the MMN concentrations using 680 or 808 nm excitation. The laser induced heat generation of the aqueous solution of MMNs was evaluated; both concentration and laser power dependent temperature increases were observed (Figure 2f and g). The photothermal effect of MMNs could increase monotonically with particle concentration and radiant energy. Interestingly, even after five cycles of laser exposure, MMNs still raised the temperature of the whole solution to the same level, suggesting that MMNs have very good photostability that allow repeated PTT treatment.

We next assessed the cell cytotoxicity, cell uptake and *in vitro* PTT effect of MMNs on U87MG cells. MMNs exhibited negligible toxicity to cells at all tested concentrations (0~500 μg/mL) (Figure 3a). The cell uptake of MMNs was evidenced by the thin-section cell TEM images (Figure 3b). Due to the high electron density, MMNs were clearly visible and distinct from the cellular matrix. Afterwards, live/dead cell staining was used to evaluate the laser triggered PTT effect of MMNs. No cell killing was found in control, laser only and MMNs only groups. Conversely, in the MMNs/laser group, most of the cells within the laser spot were destroyed and displayed a red fluorescence. The cells outside the region of laser spot remained alive, as indicated by the green fluorescence.

Encouraged by the quantitative radiolabeling yield of MMNs by isotope $^{64}$Cu, PET was employed to track *in vivo* delivery and biodistribution of $^{64}$Cu-MMNs using U87MG glioblastoma xenograft model. The decay-corrected PET images showed high tumor to background contrast (Figure 4a). The tumor uptake of $^{64}$Cu-MMNs was about 3.93 ± 0.18 percent of injected dose/gram of tissue (%ID/g) at 1 h post injection (p.i.) by a three-dimensional volume of interest (VOI) analysis method,[16] and reached a plateau (about 10 %ID/g) 18~24 h p.i. (Figure 4b). MRI and PAI were also conducted on tumor sections. As shown in Figure 4c and d, an obvious darkening effect could be observed at the tumor site over time. The PA images also showed increasing PA signal accumulation around the tumor region over time (Figure 4e). The presented results suggest MMNs as a promising contrast agent with high tumor accumulation for simultaneous PET, MRI, and PAI.

Author Manuscript Author Manuscript Author Manuscript Author Manuscript

Following *in vivo* multi-modality imaging, *in vivo* PTT treatment was carried out on the same animal model. Tumor-bearing mice were divided into four groups: control group, laser group, MMNs group, and MMNs plus laser irradiation group. When the tumors reached 60 $mm^3$, the mice were treated with an intravenous injection of MMNs (10 mg/kg, 200 μL). Based on the observations from PET, MRI, and PAI, 24 h time point was selected as the most suitable time to implement PTT. Upon localized laser irradiation (808 nm, 5 min, 0.25~1 $W/cm^2$), the *in vivo* tumor temperature change of mice administrated with MMNs was monitored by using an infrared (IR) thermal camera. As shown in Figure 5a and b, the tumor temperature changes were 15.77, 24.28, and 32.74 °C within 5 min, upon 0.25, 0.5 or 1 $W/cm^2$ 808 nm laser irradiation, respectively. Because a temperature rise of over 20 °C is enough to kill tumor cells,[1d] we thus used the fixed exposure condition (0.5 $W/cm^2$, 5 min) for *in vivo* PTT treatment. Complete tumor elimination was achieved in the MMNs/laser group, while the tumors in the other groups kept growing at the similar speed, and had to to be euthanized on day 14 due to the extensive tumor burden (Figure 5c and d). The MMNs plus laser irradiation greatly prolonged the survival of tumor-bearing mice over 30 days, without a single death or tumor reoccurrence (Figure 5d). After PTT treatment, mice showed black scars at their original sites of tumor (Figure 5e). Hematoxylin and eosin (H&E) staining images of tumor sections further evidenced the efficient photothermal effect of MMNs plus laser irradiation, showing significant cancer cell damage with nuclear membrane fragmentation and nuclei shrinkage with karyorrhexis and pyknosis that induced intensive necrosis or apoptosis.[1f] After MMNs administration and laser irradiation, main organs from different groups of mice, as seen through H&E stained images (Figure S4), showed no obvious damage or inflammation. The results manifest the capability of MMNs for photothermal imaging and photothermal tumor ablation *in vivo*.

Considering the biological function of melanin,[17] we also investigated the UV and γ irradiation protection of MMNs. We found a concentration-dependent and time-independent UV protection of MMNs at the cell level (Figure S5). The 200 μg/mL of MMNs showed much higher cell viability after 2 h UV exposure than other tested concentrations (Figure S5a). The linear regression showed a satisfactory $R^2$ value ($R^2$ = 0.9491, (Figure S5b). In the meantime, we also explored whether the UV protection of MMNs is time-dependent. We incubated the cells with MMNs (200 μg/mL) for 4 h before UV exposure, and evaluated the cell viability by CCK-8 kit assay at different time intervals. The MMNs showed better UV protection at 30 min group than other longer exposure groups (Figure S5c). The linear regression analysis reveal that the cell death increased with prolonged UV exposure (Figure S5d).

Recent studies discovered a profound protective role of melanin from ionizing radiation.[18] We therefore explored the γ-irradiation protection function of MMNs on healthy female BALB/c mice. Mice were challenged with a lethal dose of γ-irradiation using $^{60}Co$ source. The deaths of all experimental mice were recorded for Kaplan–Meier analysis. The survival rate was significantly improved in groups with intravenous injection of 50 mg/kg and 10 mg/kg of MMNs compared with PBS irradiation control ($P$ = 0.002 and $P$ = 0.038, Figure 6a), and the survival percentages were increased by 70% and 44% at day 30, respectively. Meanwhile, the median survival time was increased from 21 days (PBS irradiation control) to 30 days (10 mg/kg MMNs). On the contrary, the survival curve and media survival time

Author Manuscript Author Manuscript Author Manuscript Author Manuscript

between PBS irradiation control and 50 mg/kg MNPs groups revealed no significant difference ($P = 0.1019$, Figure 6a). In addition, we compared the body weight changes among different groups. The mice with intravenous injection of 50 mg/kg MMNs showed slowest body weight loss than other groups. On day 21, the body weight of 50 mg/kg MMNs was more than the PBS irradiation control ($P = 0.011$, Figure 5b), and treatment with MMNs (10 mg/kg and 50 mg/kg) protected the spleen as compared with PBS irradiation and MNPs groups (Figure S6). We increased the injection dose to 100 mg/kg and found no death, which suggests that the maximum tolerated dose for MMNs is over 100 mg/kg. Afterwards, the Fe content in different organs was measured by ICP-MS (Figure S7). It is not surprising to observe high uptake of MMNs in the liver and spleen. However, no obvious damage or inflammation in those oragns was found at such a high administration dose (Figure S8), as the major components of MMNs are iron and melanin, both of which are non-toxic.

These results suggest the protective role of MMNs against γ-irradiation. The main toxic substance of γ-irradiation for the living cells is reactive free radicals.[19] The radioprotective mechanism of MMNs is complicated. Other than physical shielding and quenching of cytotoxic-free radicals,[20] melanin also showed abilities in modulation of pro-survival pathways, prevention of oxidative stress and potent immunomodulation.[18, 21] Therefore, MMNs might be useful and serve as a potential radioprotector to shield the normal organs of cancer patients who are undergoing high dose radiotherapy.

In summary, we have developed a versatile biomimetic theranostic agent based on magnetic melanin nanoparticles (MMNs) for PET/MR/PA/PT multimodal imaging guided cancer PTT, UV and γ irradiation protection. MMNs were synthesized by biomimetic synthesis method using biopolymer melanin as the biotemplate, radiolabeled with $^{64}Cu$ and purified to give quantitative radiochemical yield. Both *in vitro* and *in vivo* studies further confirmed its cancer theranostic capability. *In vivo* PET imaging showed high tumor uptake of MMNs after intravenous injection (150 μCi, about 10 %ID/g at 24 h). MRI and PAI also confirmed high tumor accumulation of MMNs. Afterwards, upon mild localized laser irradiation (808 nm, 0.5 W/cm$^2$, 5 min), complete tumor elimination was achieved in MMNs administered group (10 mg/kg of MMNs). Most intriguingly, MMNs also exhibit efficient shielding against UV and γ irradiation. MMNs showed great clinical translation potential as a versatile biomimetic theranostic agent with multi-modality imaging capability and potent PTT effect, and as a potential radioprotector to shield the normal organs of cancer patients who are undergoing high dose radiotherapy.

## Supplementary Material

Refer to Web version on PubMed Central for supplementary material.

## Acknowledgments

J. L., M. W. and H. H. contributed equally to this work. This work was supported by the National Science Foundation of China (51573096, 81401465), and the Intramural Research Program (IRP) of the NIBIB, NIH.

Author Manuscript Author Manuscript Author Manuscript Author Manuscript

## References


1. a) Huynh E, Leung BY, Helfield BL, Shakiba M, Gandier JA, Jin CS, Master ER, Wilson BC, Goertz DE, Zheng G. Nat Nanotechnol. 2015; 10:325. [PubMed: 25822929] b) Lovell JF, Jin CS, Huynh E, Jin H, Kim C, Rubinstein JL, Chan WC, Cao W, Wang LV, Zheng G. Nat Mater. 2011; 10:324. [PubMed: 21423187] c) Huang P, Lin J, Wang X, Wang Z, Zhang C, He M, Wang K, Chen F, Li Z, Shen G, Cui D, Chen X. Adv Mater. 2012; 24:5104. [PubMed: 22718562] d) Huang P, Lin J, Li W, Rong P, Wang Z, Wang S, Wang X, Sun X, Aronova M, Niu G, Leapman RD, Nie Z, Chen X. Angew Chem Int Ed Engl. 2013; 52:13958. [PubMed: 24318645] e) Rai P, Mallidi S, Zheng X, Rahmanzadeh R, Mir Y, Elrington S, Khurshid A, Hasan T. Adv Drug Deliv Rev. 2010; 62:1094. [PubMed: 20858520] f) Huang P, Rong P, Lin J, Li W, Yan X, Zhang MG, Nie L, Niu G, Lu J, Wang W, Chen X. J Am Chem Soc. 2014; 136:8307. [PubMed: 24842342] g) Huang P, Gao Y, Lin J, Hu H, Liao HS, Yan X, Tang Y, Jin A, Song J, Niu G, Zhang G, Horkay F, Chen X. ACS nano. 2015h) Song J, Huang P, Duan H, Chen X. Acc Chem Res. 2015; 48:2506. [PubMed: 26134093]
2. a) Shin TH, Choi Y, Kim S, Cheon J. Chem Soc Rev. 2015; 44:4501. [PubMed: 25652670] b) Rieffel J, Chen F, Kim J, Chen G, Shao W, Shao S, Chitgupi U, Hernandez R, Graves SA, Nickles RJ, Prasad PN, Kim C, Cai W, Lovell JF. Adv Mater. 2015; 27:1785. [PubMed: 25640213] c) Ma J, Huang P, He M, Pan L, Zhou Z, Feng L, Gao G, Cui D. J Phys Chem B. 2012; 116:14062. [PubMed: 23134318] d) Song XR, Wang X, Yu SX, Cao J, Li SH, Li J, Liu G, Yang HH, Chen X. Adv Mater. 2015; 27:3285. [PubMed: 25885638] e) Huang P, Rong P, Jin A, Yan X, Zhang MG, Lin J, Hu H, Wang Z, Yue X, Li W, Niu G, Zeng W, Wang W, Zhou K, Chen X. Adv Mater. 2014; 26:6401. [PubMed: 25123089] f) Lin J, Wang S, Huang P, Wang Z, Chen S, Niu G, Li W, He J, Cui D, Lu G, Chen X, Nie Z. ACS nano. 2013; 7:5320. [PubMed: 23721576]
3. a) Lee H, Shin TH, Cheon J, Weissleder R. Chem Rev. 2015b) Lee N, Yoo D, Ling D, Cho MH, Hyeon T, Cheon J. Chem Rev. 2015c) Reddy LH, Arias JL, Nicolas J, Couvreur P. Chem Rev. 2012; 112:5818. [PubMed: 23043508] d) Yoo D, Lee JH, Shin TH, Cheon J. Acc Chem Res. 2011; 44:863. [PubMed: 21823593]
4. Huang P, Li Z, Lin J, Yang D, Gao G, Xu C, Bao L, Zhang C, Wang K, Song H, Hu H, Cui D. Biomaterials. 2011; 32:3447. [PubMed: 21303717]
5. Chakravarty R, Valdovinos HF, Chen F, Lewis CM, Ellison PA, Luo H, Meyerand ME, Nickles RJ, Cai W. Adv Mater. 2014; 26:5119. [PubMed: 24944166]
6. Xie J, Chen K, Huang J, Lee S, Wang J, Gao J, Li X, Chen X. Biomaterials. 2010; 31:3016. [PubMed: 20092887]
7. Xue S, Wang Y, Wang M, Zhang L, Du X, Gu H, Zhang C. Int J Nanomedicine. 2014; 9:2527. [PubMed: 24904212]
8. Hwang do W, Ko HY, Kim SK, Kim D, Lee DS, Kim S. Chem Eur J. 2009; 15:9387. [PubMed: 19658128]
9. a) Gleich B, Weizenecker J. Nature. 2005; 435:1214. [PubMed: 15988521] b) Borgert J, Schmidt JD, Schmale I, Bontus C, Gleich B, David B, Weizenecker J, Jockram J, Lauruschkat C, Mende O, Heinrich M, Halkola A, Bergmann J, Woywode O, Rahmer J. Biomed Tech (Berl). 2013; 58:551. [PubMed: 24025718]
10. Mehrmohammadi M, Shin TH, Qu M, Kruizinga P, Truby RL, Lee JH, Cheon J, Emelianov SY. Nanoscale. 2013; 5:11179. [PubMed: 24080913]
11. Qu M, Mehrmohammadi M, Emelianov S. Small. 2011; 7:2858. [PubMed: 21910248]
12. Enochs WS, Petherick P, Bogdanova A, Mohr U, Weissleder R. Radiology. 1997; 204:417. [PubMed: 9240529]
13. a) Larsson B, Tjalve H. Acta Physiol Scand. 1978; 104:479. [PubMed: 726939] b) Fan Q, Cheng K, Hu X, Ma X, Zhang R, Yang M, Lu X, Xing L, Huang W, Gambhir SS, Cheng Z. J Am Chem Soc. 2014; 136:15185. [PubMed: 25292385] c) Zhang R, Fan Q, Yang M, Cheng K, Lu X, Zhang L, Huang W, Cheng Z. Adv Mater. 2015; 27:5063. [PubMed: 26222210] d) Ju KY, Lee Y, Lee S, Park SB, Lee JK. Biomacromolecules. 2011; 12:625. [PubMed: 21319809]
14. Liu Y, Ai K, Liu J, Deng M, He Y, Lu L. Adv Mater. 2013; 25:1353. [PubMed: 23280690]
15. Zhao Z, Zhou Z, Bao J, Wang Z, Hu J, Chi X, Ni K, Wang R, Chen X, Chen Z, Gao J. Nat Commun. 2013; 4:2266. [PubMed: 23903002]

Author Manuscript Author Manuscript Author Manuscript Author Manuscript

16. Hu H, Huang P, Weiss OJ, Yan X, Yue X, Zhang MG, Tang Y, Nie L, Ma Y, Niu G, Wu K, Chen X. Biomaterials. 2014; 35:9868. [PubMed: 25224367]
17. Hill HZ. BioEssays: news and reviews in molecular, cellular and developmental biology. 1992; 14:49.
18. Rageh MM, El-Gebaly RH, Abou-Shady H, Amin DG. Mol Cell Biochem. 2015; 399:59. [PubMed: 25300618]
19. a) Hosseinimehr SJ. Drug Discov Today. 2007; 12:794. [PubMed: 17933679] b) Hosseinimehr SJ. Cancer Biother Radiopharm. 2009; 24:723. [PubMed: 20025553]
20. a) Dadachova E, Casadevall A. Curr Opin Microbiol. 2008; 11:525. [PubMed: 18848901] b) Dadachova E, Bryan RA, Howell RC, Schweitzer AD, Aisen P, Nosanchuk JD, Casadevall A. Pigment Cell Melanoma Res. 2008; 21:192. [PubMed: 18426412] c) Dadachova E, Bryan RA, Huang X, Moadel T, Schweitzer AD, Aisen P, Nosanchuk JD, Casadevall A. PloS one. 2007; 2:e457. [PubMed: 17520016]
21. a) Schweitzer AD, Howell RC, Jiang Z, Bryan RA, Gerfen G, Chen CC, Mah D, Cahill S, Casadevall A, Dadachova E. PloS one. 2009; 4:e7229. [PubMed: 19789711] b) Kunwar A, Adhikary B, Jayakumar S, Barik A, Chattopadhyay S, Raghukumar S, Priyadarsini KI. Toxicol Appl Pharmacol. 2012; 264:202. [PubMed: 22968190]

Author Manuscript Author Manuscript Author Manuscript Author Manuscript

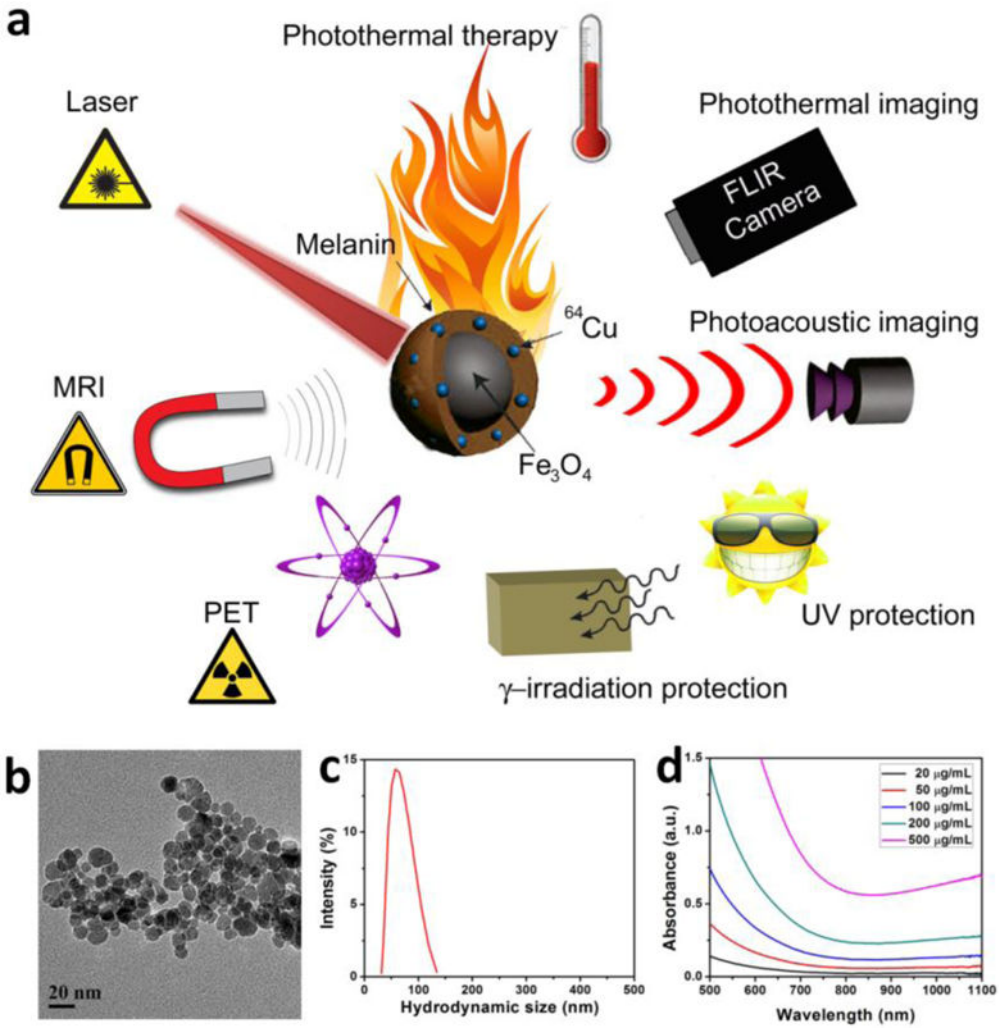


**Figure 1.**

(a) Schematic illustration of radionuclide $^{64}$Cu labeled magnetic melanin nanopaticles ($^{64}$Cu-MMNs) as versatile biomimetic theranostics for multimodal imaging guided photothermal therapy, UV and γ irradiation protection. (b) TEM image of MMNs. (c) Size distribution of MMNs in aqueous solution measured by DLS. (d) UV-vis-NIR absorption spectra of MMNs at different concentrations.

Author Manuscript Author Manuscript Author Manuscript Author Manuscript

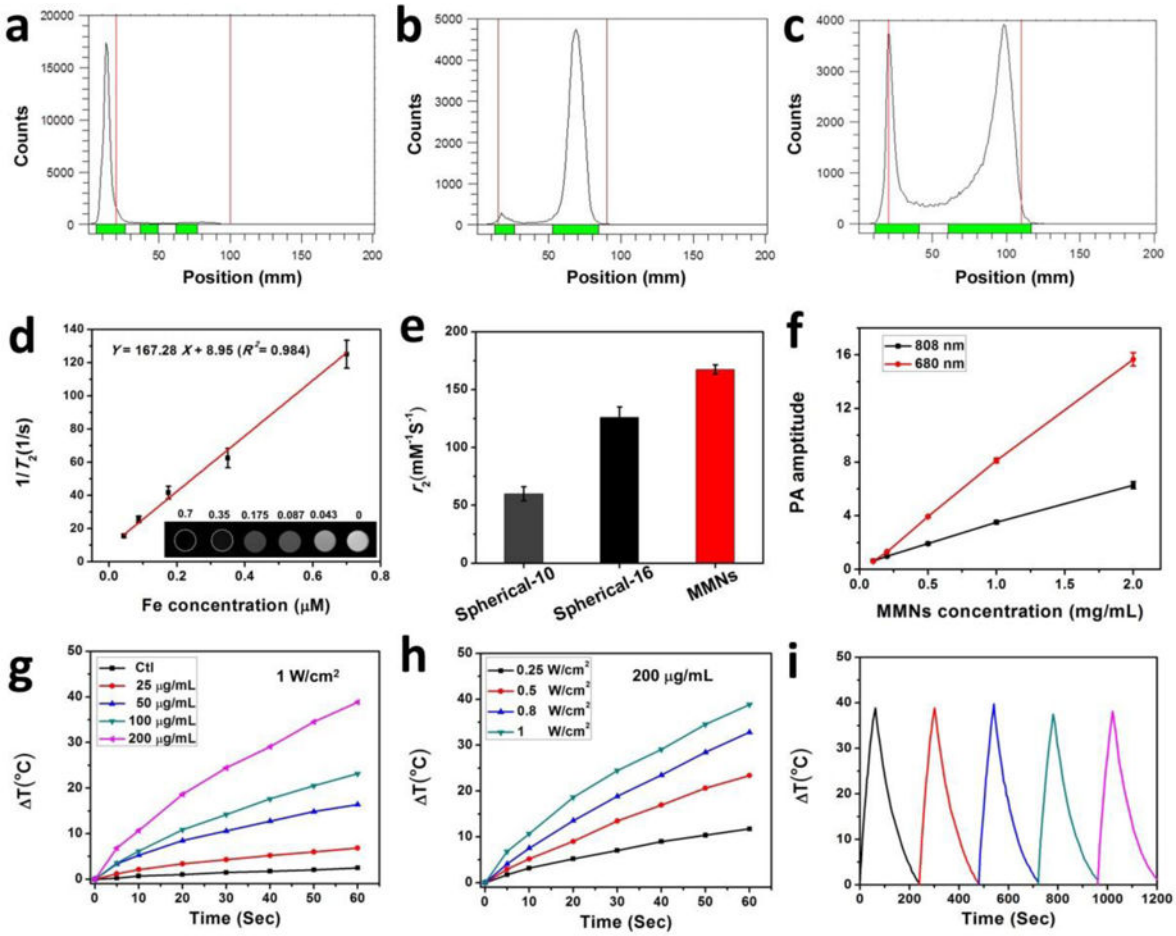


**Figure 2.**

(a–c) Radio TLC chromatograms of $^{64}$Cu-MMNs (a), free $^{64}$Cu (b), and MNPs (c). (d) $1/T_2$ vs. Fe concentration (μM) curve of MMNs in agarose gel. The slope, i.e. the $r_2$ value, was evaluated to be 167.28 $mM^{-1}$ $s^{-1}$. Inset: The corresponding $T_2$-weighted MRI image. (e) The $r_2$ values of spherical-10 (10 nm), spherical-16 (16 nm), and MMNs. (f) PA signals of MMNs as a function of concentration under 680 and 808 nm excitation, respectively. (g–h) NIR laser-induced heat generation of aqueous solution of MMNs: (g) with the same laser power density of 1 W/cm$^2$ and different concentrations. (h) with same concentration (200 μg/mL) and different laser power densities (0.25~1 W/cm$^2$). (i) Plot of temperature change ($_{\Delta}$T) of MMNs solution (200 μg/mL) irradiated by an 808 nm laser (1 W/cm$^2$) for five on/off cycles (on: 1 min, off: 3 min).

Author Manuscript Author Manuscript Author Manuscript Author Manuscript

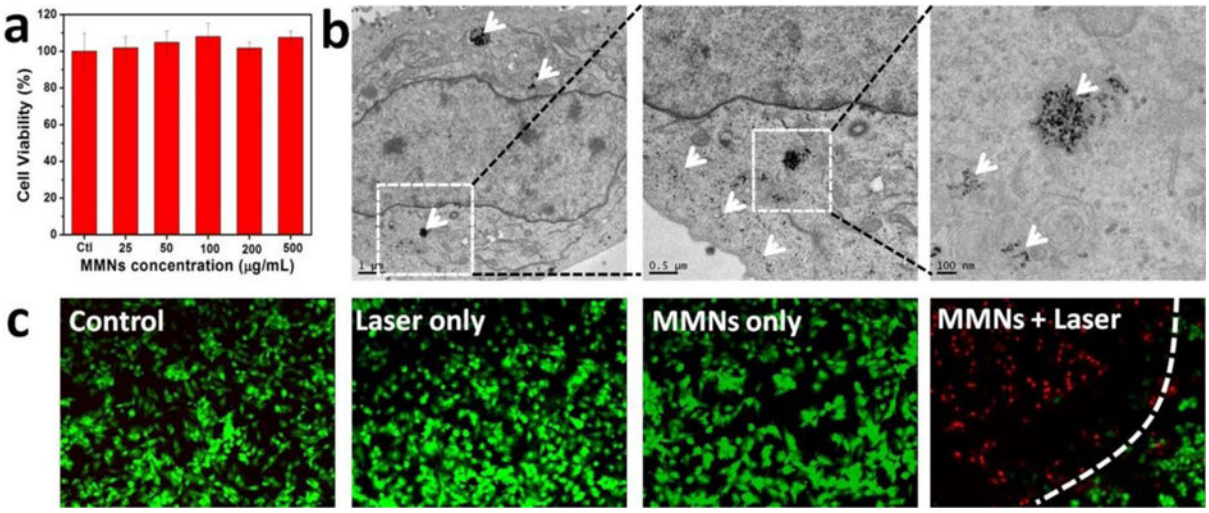


**Figure 3.** ***In vitro*** **cell experiments**

a) Cell cytotoxicity of MMNs to U87MG cells incubated with 0~500 μg/mL MMNs for 24 h. b) TEM images taken on U87MG cells incubated with 100 μg/mL MMNs for 12 h. White arrows denote the MMNs or their aggregates. c) Fluorescence images of Calcein AM (live cells, green fluorescence) and propidium iodide (PI) (dead cells, red fluorescence) co-stained U87MG cells incubated with MMNs (100 μg/mL) for 12 h after laser irradiation (808 nm, 1 W/cm$^2$, 3 min).

Author Manuscript Author Manuscript Author Manuscript Author Manuscript

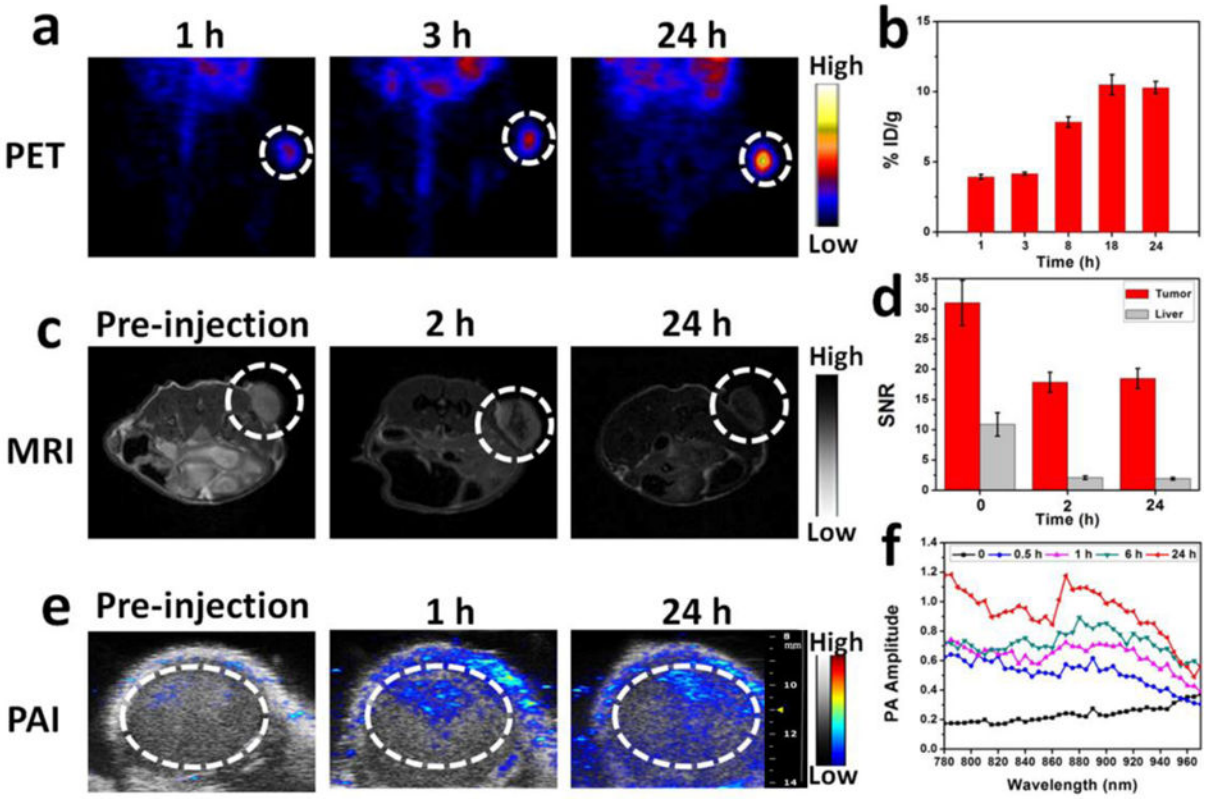


**Figure 4.** ***In vivo*** **multi-modality imaging**

(a) PET images of U87MG tumor (white dotted circle) bearing mice at different times after intravenous injection of $^{64}$Cu-MMNs. (b) Tumor uptake of $^{64}$Cu-MMNs, measured by VOIs. Data were average decay-corrected to the time of injection, presented as %ID/g. (c) MRI images of U87MG tumor (white dotted circle) before and after intravenous injection of $^{64}$Cu-MMNs. (d) Quantitative analysis of enhanced MR signal of U87MG tumor and liver before and after intravenous injection of $^{64}$Cu-MMNs. (e) PA images of U87MG tumor before and after intravenous injection of $^{64}$Cu-MMNs. The white dotted circles indicate the region of interest in the tumors. (f) PA spectra of U87MG tumor before and after intravenous injection of $^{64}$Cu-MMNs.

Author Manuscript Author Manuscript Author Manuscript Author Manuscript

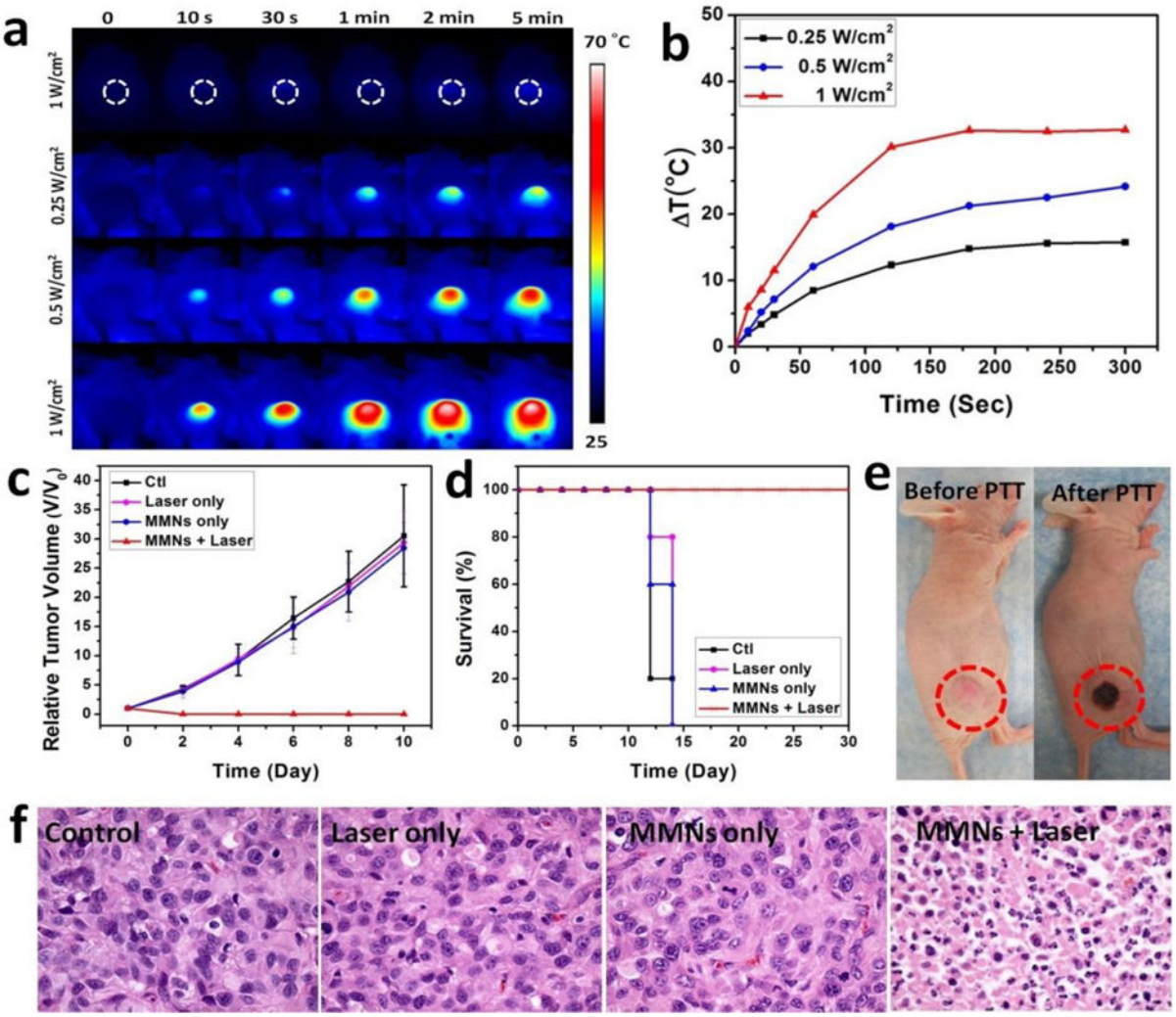


**Figure 5.** ***In vivo*** **photothermal therapy**

(a) Thermographic images of U87MG tumor-bearing mice at 24 h post-injection of MMNs (808 nm, 5 min, 0.25~1 W/cm$^2$). (b) The corresponding temperature changes (ΔT) of U87MG tumors upon laser irradiation. (c) Tumor growth curves of different groups of U87MG tumor-bearing mice after treatment. Tumor volumes were normalized to their initial sizes. Error bars represent the standard deviations of 5 mice per group. (d) Survival curves of mice bearing U87MG tumor after various treatments. (e) Photographs of U87MG tumor-bearing mice after PTT treatment. (f) H&E staining images of tumor sections harvested from U87MG tumor-bearing mice with various treatments.

Author Manuscript Author Manuscript Author Manuscript Author Manuscript

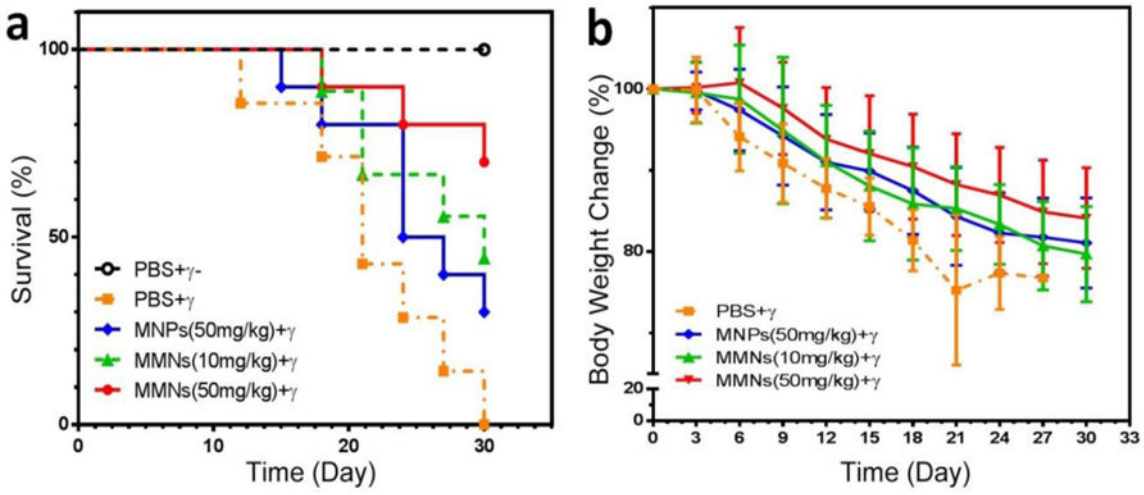


**Figure 6. In vivo γ irradiation protection**

(a) Survival curves of mice after various treatments indicated. (b) Body weight changes of mice after various treatments indicated.